Helioseismology of the "Average" Supergranule

A.C. Birch[1], T. L. Duvall Jr. [2], L. Gizon[3], J. Jackiewicz[3]

1. CoRA, NWRA, Boulder, CO
aaronb@cora.nwra.com
2. Laboratory for Solar and Space Physics
NASA/Goddard Space Flight Center
3. Max-Planck-Institut fuer Sonnensystemforschung, Germany

Abstract

We show time-distance travel times averaged over roughly ten thousand supergranules. The statistical (realization) noise in these measurements is substantially smaller than the noise associated with a single supergranule. By both forward modeling and inversions we investigate the range of flows that are compatible with these travel times.

The data & feature selection

- 68 hours of MDI/*SOHO* full-disk Dopplergrams (Scherrer *et al.*, 1995)
- Use time-distance helioseismology to measure the f-mode divergence signal (e.g. Duvall and Gizon, 2000)
- Identify supergranules in divergence signal
- Average travel times (Duvall *et al.*, 1993) around centers of supergranules (see Fig. 1)

Measurement geometry

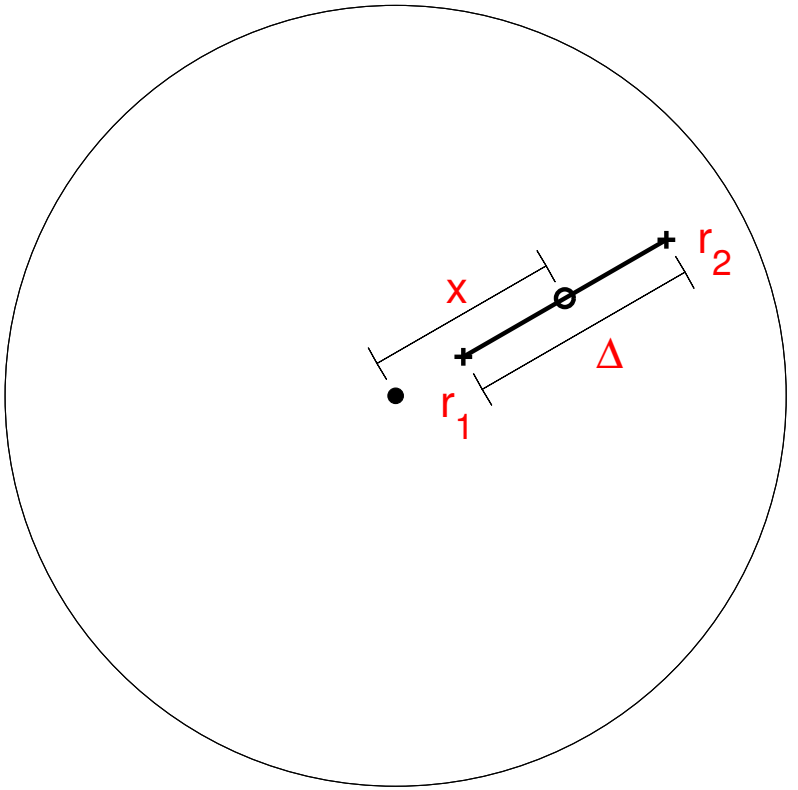

Figure 1: Geometry for measuring travel times. The offset from the center of the supergranule is x and $\Delta = \|r_2 - r_1\|$. The travel times from $r_2 \rightarrow r_1$ and $r_1 \rightarrow r_2$ are measured. These times are averaged over all azimuths from the center of the supergranule and over 10^4 supergranules.

F-mode travel times

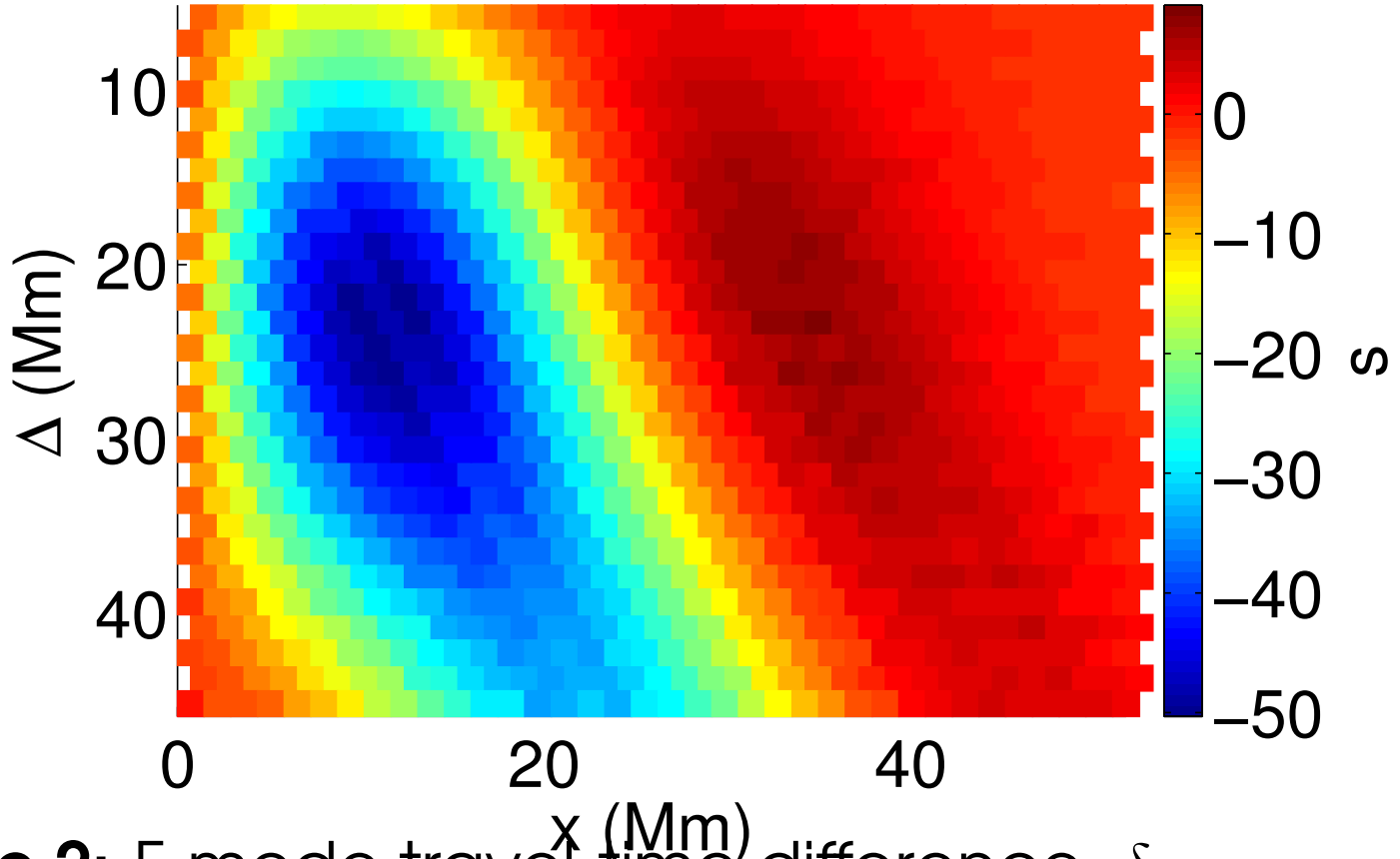

Figure 2: F-mode travel-time difference, $\delta\tau = \tau_{\rm out} - \tau_{\rm in}$ (in seconds) as a function of offset, x, and distance, Δ.

Noise Estimate

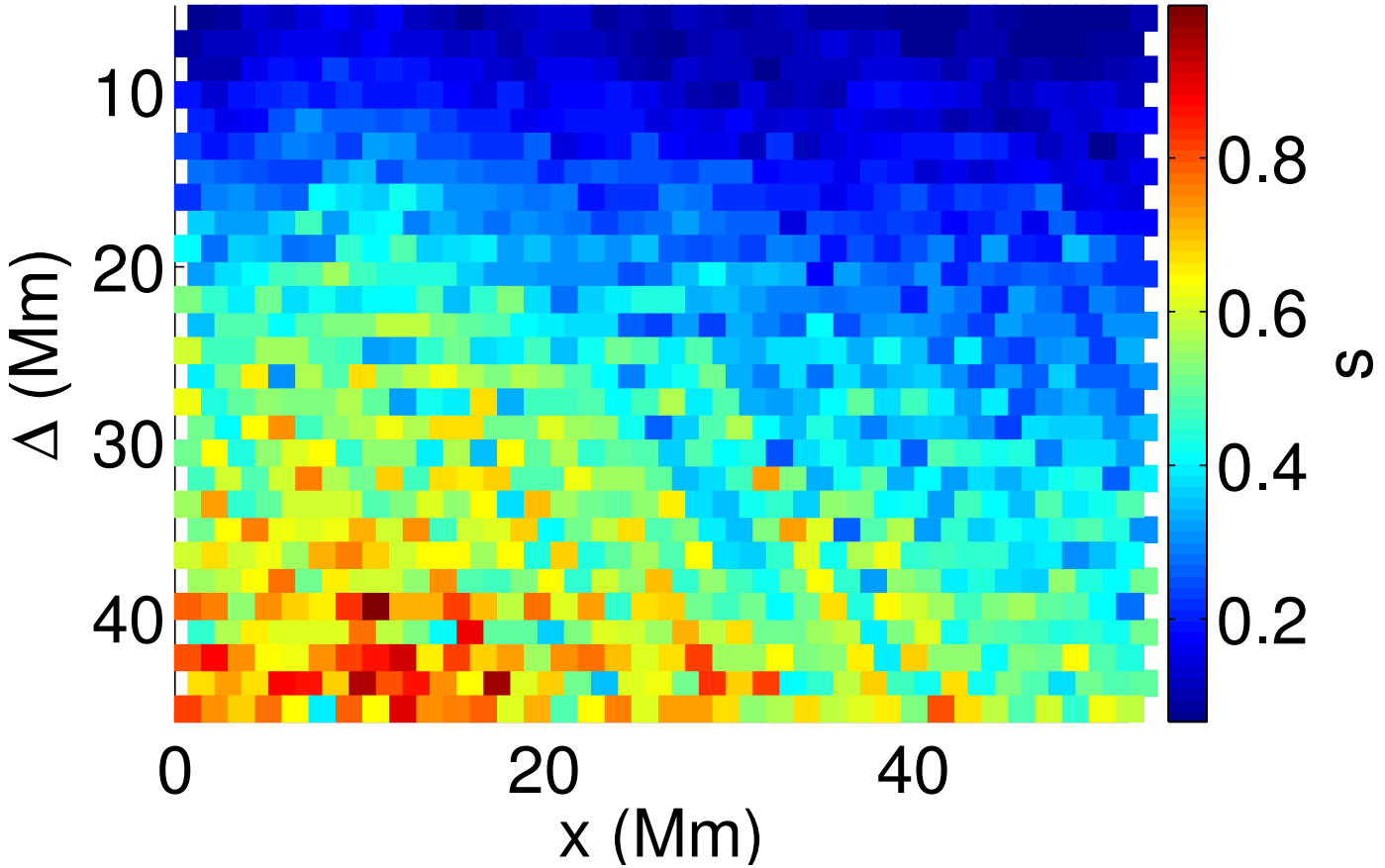

Figure 3: Noise level, estimated from the scatter in the data, in the travel-time differences shown in Figure 2, as a function of offset, x, and distance, Δ.

Example f-mode kernel

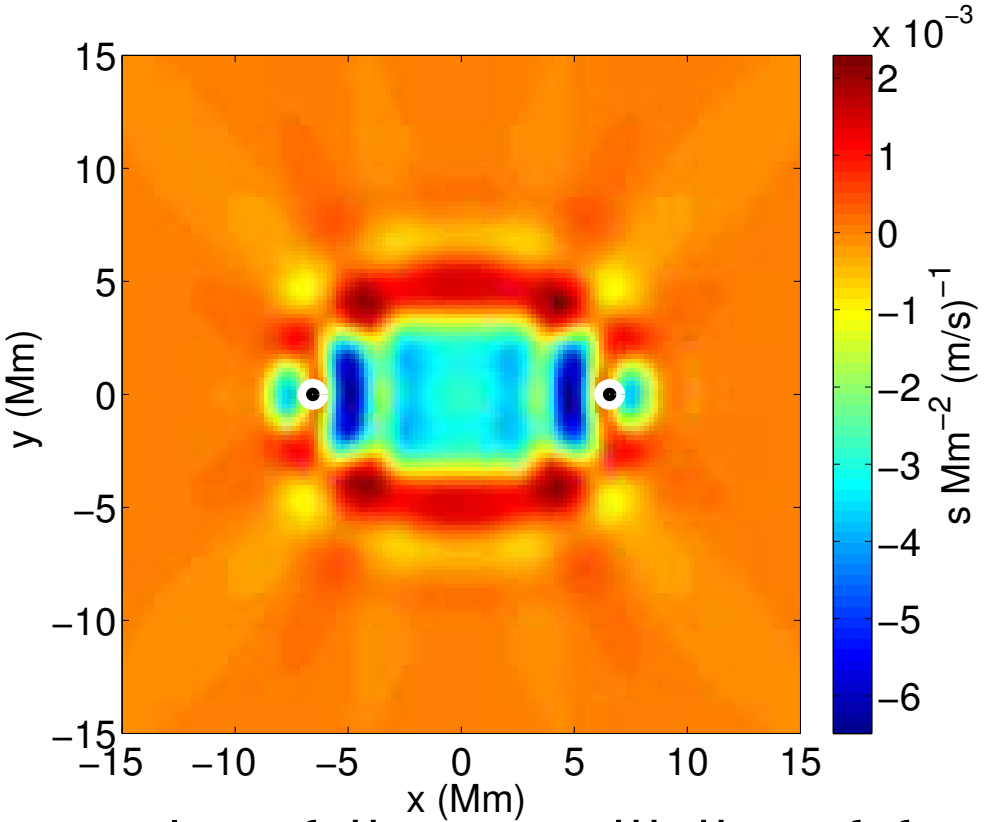

Figure 4: Example of the sensitivity of f-mode travel-time differences to flows in the $+\hat{\mathbf{x}}$ direction and for a separation of $\Delta = \|\boldsymbol{r}_2 - \boldsymbol{r}_1\| = 13.1$ Mm. The observation points $\boldsymbol{r}_1$ and $\boldsymbol{r}_2$ are located at the black dots, $(x, y) = (\pm\Delta/2, 0)$.

F-mode kernels

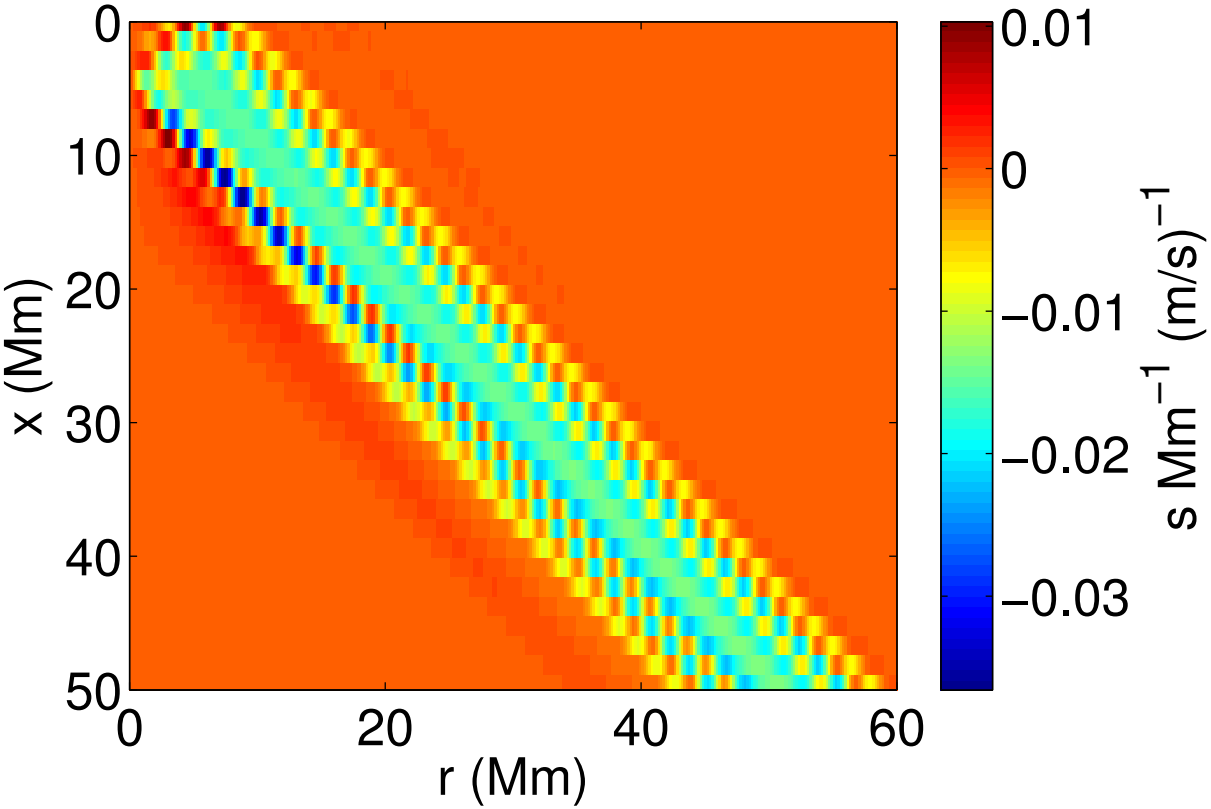

Figure 5: Sensitivity of azimuthal averages of f-mode travel-time differences to radial flows $\boldsymbol{v} = v(r)\hat{r}$, as a function of distance from the center of the supergranule, x, and the distance from the center of the supergranule, r. This example is for $\Delta = 13.1$ Mm.

A forward model

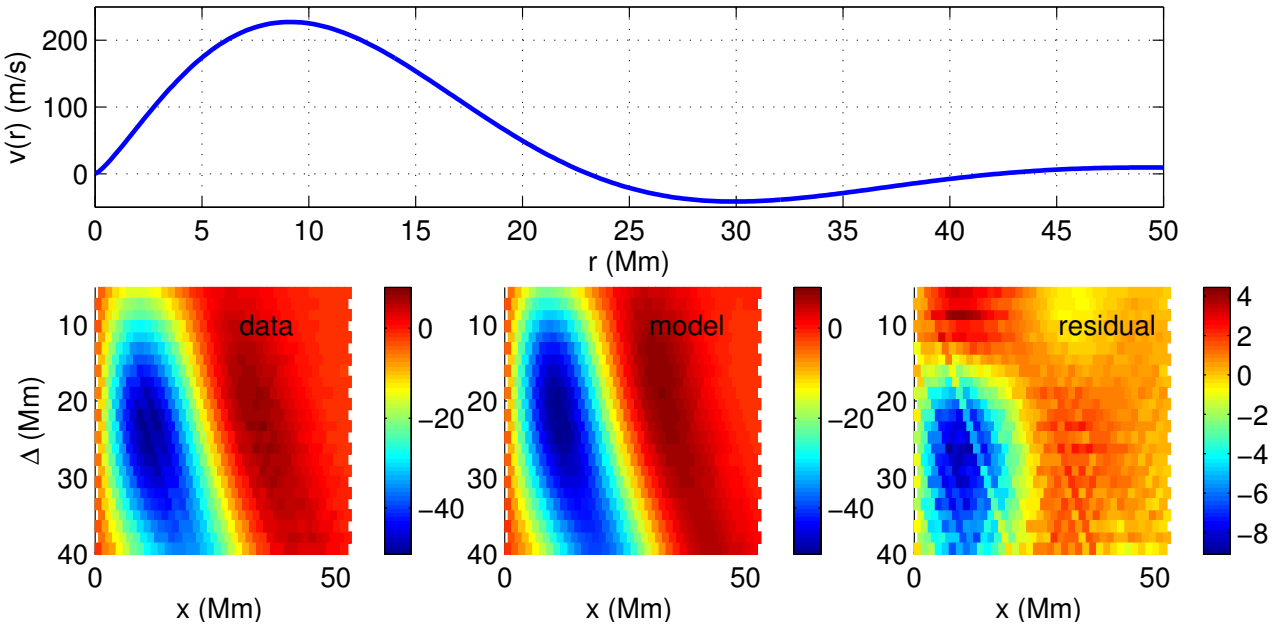

Figure 6: Forward modeling to estimate the flow $v(r)$ that is compatible with the data. We search for a flow of the form $v(r) = r^n J_1(kr)e^{-r/L}$ where n, k, L are free parameters. We find the best fit at $(n, k, L) = (0.4, 0.17\ \mathrm{Mm}^{-1}, 13\ \mathrm{Mm})$ (top panel). The bottom three panels show the measured travel times (left), the model travel times (middle), and residuals (right). In the lower panels the units are seconds.

RLS inversion

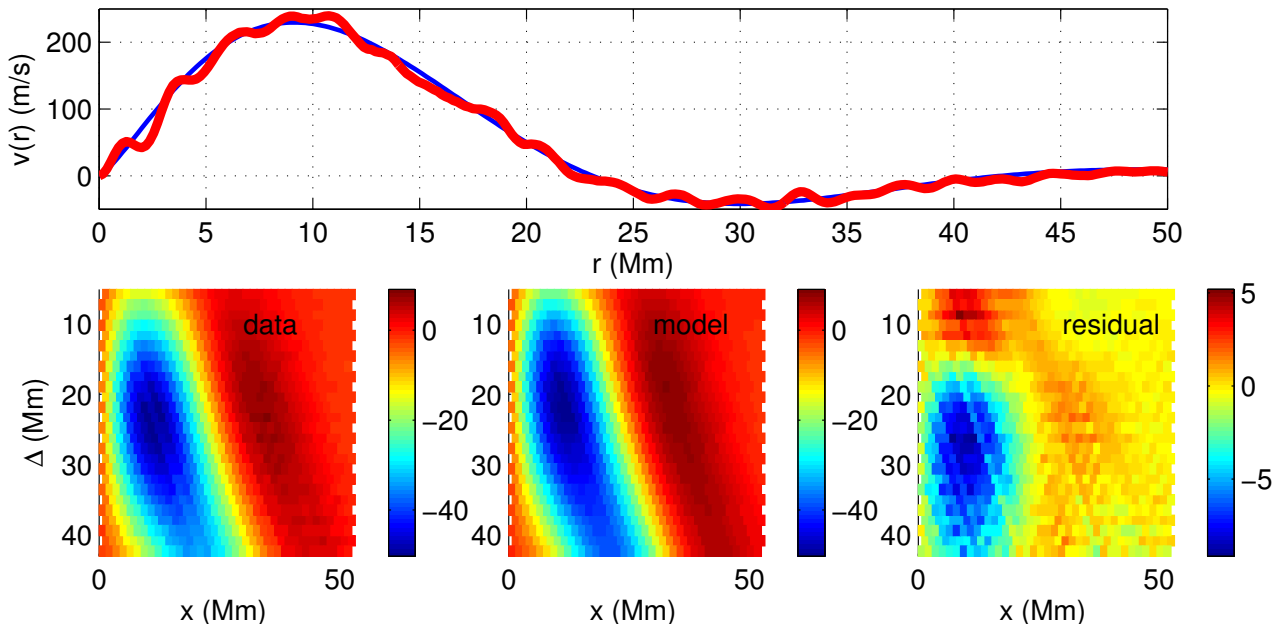

Figure 7: RLS inversion for $v(r)$ (red line in top panel). Also shown is the forward modeling result (blue line in top panel). The bottom panels shows the observed travel times (left), the model travel times corresponding to the RLS inversion result (middle), and the residuals (right). In the lower panels the units are seconds.

RLS inversions for each Δ

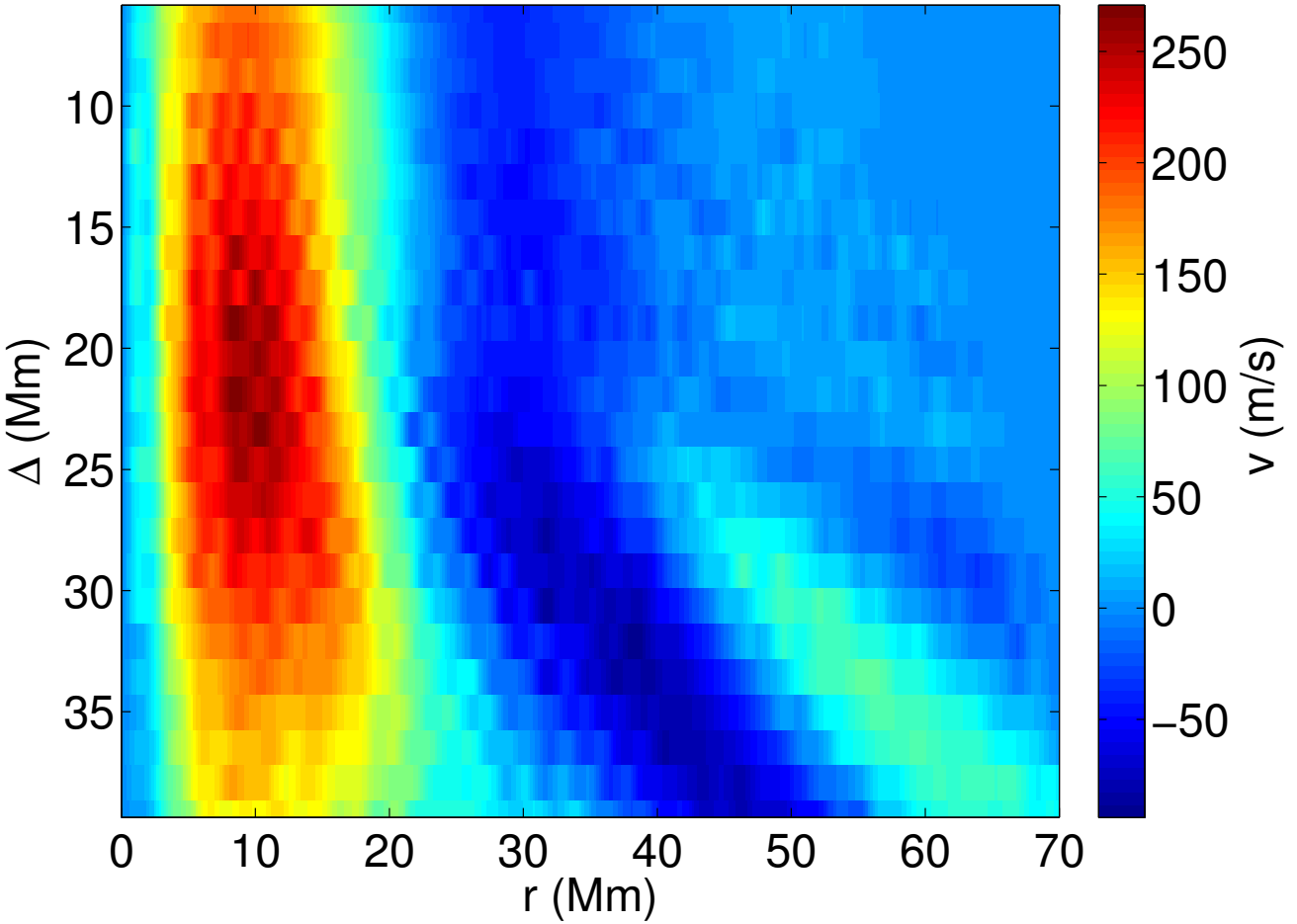

Figure 8: RLS inversions for $v(r)$ at fixed Δ. At each distance a separate inversion is used to determine $v(r)$, using only the travel times measured at that Δ.

P-mode travel times

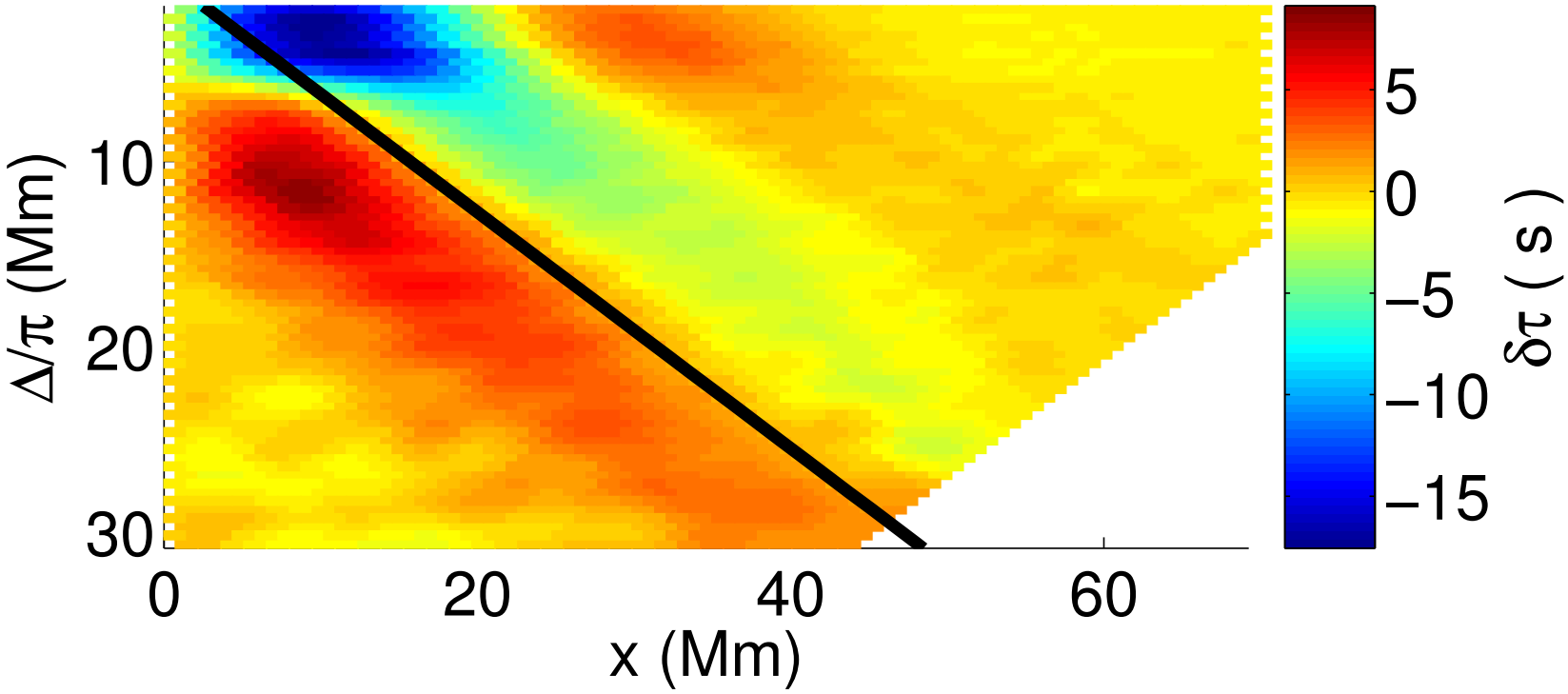

Figure 9: Travel-time differences, $\delta\tau = \tau_{\rm out} - \tau_{\rm in}$, for p modes, as functions of approximate lower turning point, Δ/π, and offset, x from the supergranule center. The heavy black line corresponds to rays that begin at the center of the supergranule.

P-mode Noise Estimate

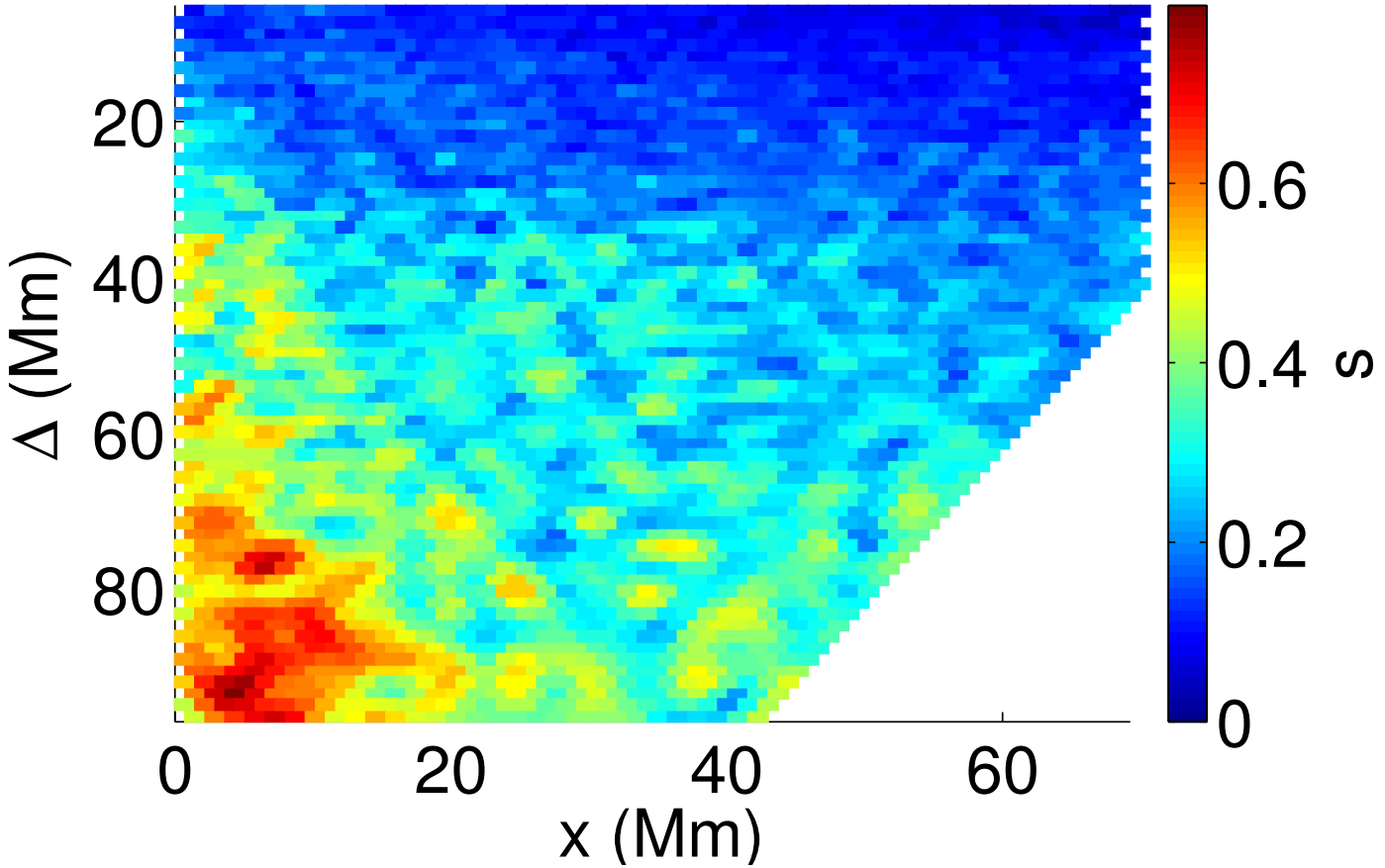

Figure 10: Noise level, estimated from the scatter in the data, in the travel-time differences shown in Figure 9, as a function of offset, x, and distance, Δ.

Ray coverage

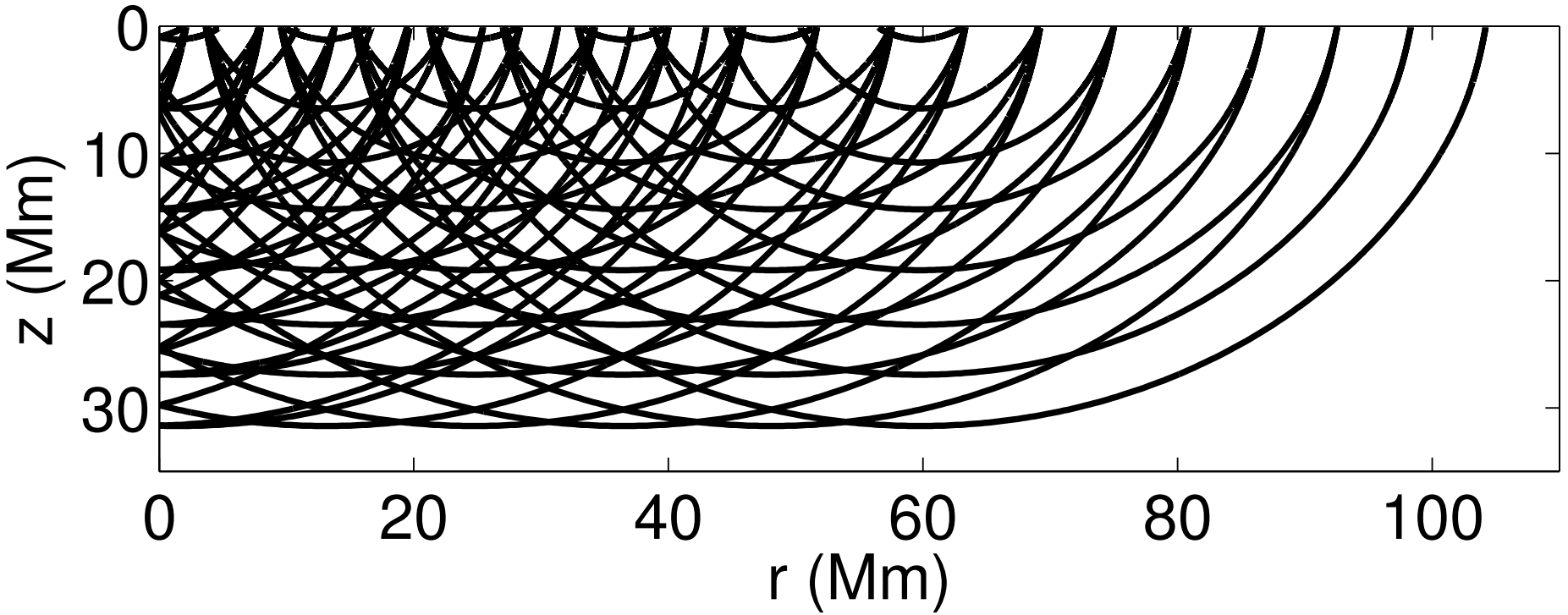

Figure 11: A small sample, about 2%, of the ray paths represented in Figure 9. Depth is z and horizontal distance from the center of the supergranule is r.

A simple forward model

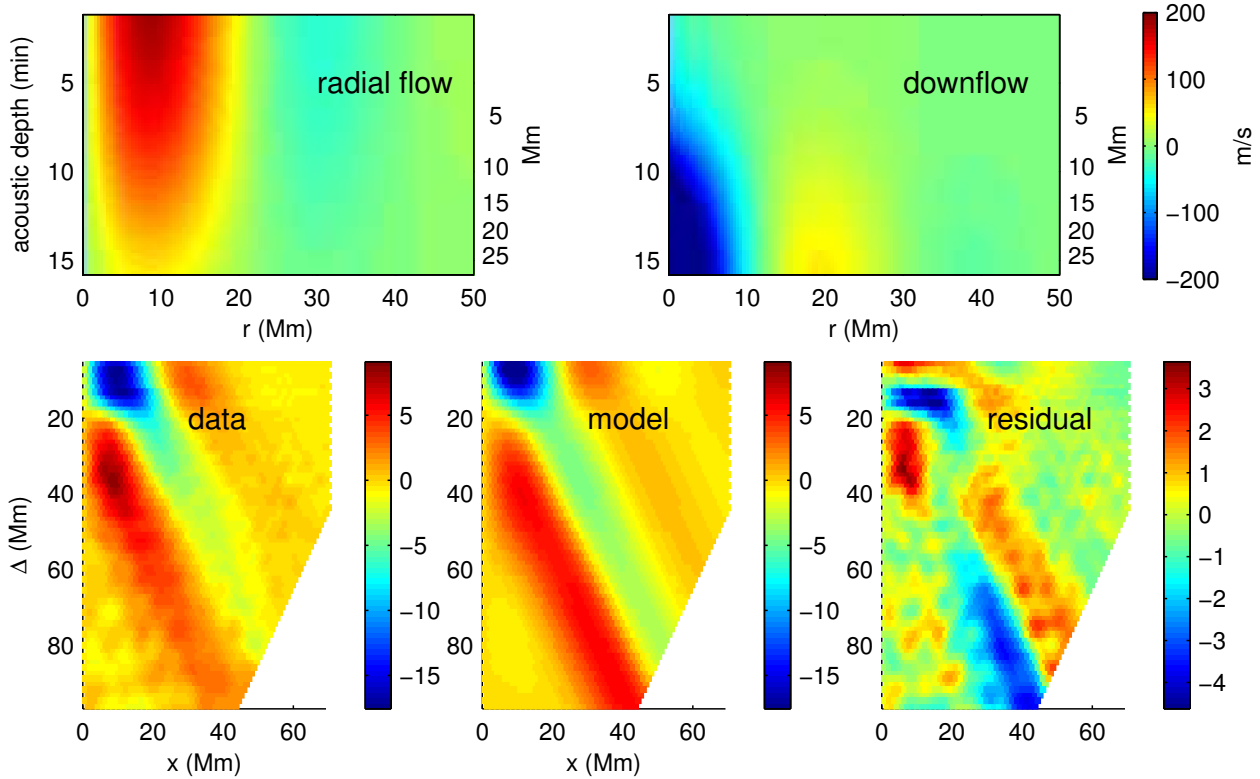

Figure 12: An example forward model. The radial flow (top left panel) is of the form $v_r = J_1(kr)e^{-r/L}e^{-z/D}$ and the vertical flow (top right panel) is determined from mass conservation. The best fit to the data is found for $(k, L, D) = (.17\ \mathrm{Mm}^{-1}, 19\ \mathrm{Mm}, 24\ \mathrm{Mm})$. The lower panels shows the data, model times, and residuals.

Conclusions

- f-modes:
  - even with RLS inversion, there is a clear pattern in the residuals.
  - multiple scattering effects ?
  - significant depth dependence ?
- p-modes:
  - only preliminary work so far
  - The data promise to strongly constrain the subsurface flow pattern

Future work

- Ray theory inversions for the p-mode data
- Treat full error covariance, currently only the diagonal part of the covariance is employed
- Inversions using Born approximation kernels for p-mode and f-modes
- 2d (depth,radius) inversions of f-mode data
- Joint inversion of p- and f-mode data

References

Duvall, T. L., J., Gizon, L., 2000, "Time-Distance Helioseismology with f Modes as a Method for Measurement of Near-Surface Flows", Sol. Phys., **192**, 177–191

Duvall, T. L., Jefferies, S. M., Harvey, J. W., Pomerantz, M. A., 1993, "Time-distance helioseismology", Nature, **362**, 430–432

Scherrer, P. H., Bogart, R. S., Bush, R. I., Hoeksema, J. T., Kosovichev, A. G., Schou, J., Rosenberg, W., Springer, L., Tarbell, T. D., Title, A., Wolfson, C. J., Zayer, I., MDI Engineering Team, 1995, "The Solar Oscillations Investigation - Michelson Doppler Imager", Sol. Phys., **162**, 129–188